Available online at www.sciencedirect.com
ScienceDirect
Journal of Molecular Catalysis A: Chemical 271 (2007) 46–56
JOURNAL OF MOLECULAR CATALYSIS A: CHEMICAL
www.elsevier.com/locate/molcata

Silicotungstic acid/zirconia immobilized on SBA-15 for esterifications

Dhanashri P. Sawant [a], A. Vinu [b], S.P. Mirajkar [a], F. Lefebvre [c], K. Ariga [d], S. Anandan [b], T. Mori [b], C. Nishimura [e], S.B. Halligudi [a,*]

[a] *Inorganic Chemistry & Catalysis Division, National Chemical Laboratory, Pune 411008, Maharashtra, India*
[b] *Nano-ionics Materials Group, National Institute for Materials Science, 1-1, Namiki, Tsukuba, Japan*
[c] *Laboratoire de Chimie Organométallique de Surface, CNRS-CPE, Villeurbanne Cedex, France*
[d] *Supermolecules Group, National Institute for Materials Science, 1-1, Namiki, Tsukuba, Japan*
[e] *Hydrogen Purification Materials Group, National Institute for Materials Science, 1-1, Namiki, Tsukuba, Japan*

Received 22 December 2006; received in revised form 20 February 2007; accepted 20 February 2007
Available online 24 February 2007

Abstract

A simple wet-impregnation method and controlled calcination process was used for preparing nano-sized silicotungstic acid (STA) supported on zirconia embedded inside the various mesoporous silicas such as SBA-15, MCM-41 and MCM-48. Catalysts with different (%) STA loadings were also synthesized and characterized by XRD, N_2 adsorption–desorption, TEM, ^{29}Si-MAS NMR, FT-Raman spectroscopic techniques. The acidic behavior of the catalysts was studied by TPD of ammonia and FT-IR pyridine adsorption technique. The effect of calcination temperature on the textural parameters of the catalysts and the integrity of STA on the surface of the catalyst were also examined. Moreover, the performance of these catalysts was investigated in the esterification of isoamyl alcohol (IAA) with acetic acid (AA). Catalytic activities were correlated with the acidity of the catalysts. Effects of reaction parameters such as mole ratio of reactants, reaction temperature, catalyst concentration and reusability of the catalyst were studied to get higher substrate conversions and product selectivities. Among the catalysts, 15 wt.% STA/22.4 wt.% ZrO_2/SBA-15 calcined at 1123 K was found to be the most active and acidic catalyst, showing higher conversion and selectivity than neat 15 wt.% STA/ZrO_2 in esterification of IAA by AA. The reaction was found to be heterogeneously catalyzed and no contribution from homogeneous (leached) STA into the medium under the reaction conditions was observed.

Keywords: STA/ZrO_2; SBA-15; Wet-impregnation; Isoamyl acetate; Esterification

1. Introduction

A wide category of organic compounds ranging from aliphatic to aromatic esters, are generally used as plasticizers, solvents, perfumery, fragrant chemicals and precursors for a wide range of pharmaceuticals, agrochemicals and fine chemicals [1]. Esterification of alcohols by carboxylic acids is one of the most important reactions in organic synthesis [2] which has been investigated over many solid acid catalysts such as immobilized lipase [3–6], Y-type zeolite [7] and immobilized Rhizomucor miehei [8]. Particularly the esterification of isoamyl alcohol (IAA) with acetic acid (AA) in gaseous phase has been studied using tungstophosphoric acid (TPA) supported on different carriers such as silica materials, carbon, alumina, Cs or K salts, Al-MCM-41, cation-exchange resin Purolite CT-175 under vapour and liquid phase conditions [9–12]. A series of ecofriendly solid acid catalyst with STA supported on hydrous zirconia have been synthesized using impregnation method and their catalytic properties have been evaluated for the esterification of 1° alcohol (*n*-butanol, *iso*-butanol) and 2° alcohol (2-butanol, cyclohexanol) [13].

Esterification reactions have been extensively studied in presence of Keggin and Wells-Dawson heteropoly acids as homogeneous catalysts [14–16]. The catalytic activities of heteropoly acids (HPAs) usually follow the order of their acid strengths, as expected for Brönsted acid catalysis. Maksimov and Kozhevnikov showed that Keggin acids such as TPA and STA are two to four times more active than the conventional catalysts per unit proton site [17]. Interestingly, the Wells-Dawson acid, $H_6[P_2W_{18}O_{62}]$, shows two times higher activity than TPA. HPAs supported on carbon catalysts have been widely used in liquid-phase esterification and related reactions in polar media because

* Corresponding author. Tel.: +91 20 25902107; fax: +91 20 25902634.
E-mail address: sb.halligudi@ncl.res.in (S.B. Halligudi).

1381-1169/$ – see front matter © 2007 Elsevier B.V. All rights reserved.
doi:10.1016/j.molcata.2007.02.029

the surface area of activated carbon is quite high, which enhances the adsorption of HPAs [18]. Carbon-supported TPA catalyst has also been utilized for the esterification of phthalic anhydride with C_8–C_{10} alcohols performed at the reaction temperature of 373–393 K to yield dialkyl phthalates. Dupont and Lefebvre [19] studied the esterification of propanoic acid by butanol or 2-ethylhexanol catalyzed by STA and TPA pure or supported on carbon. Unfortunately, the carbon-supported HPAs register a rather low catalytic activity because of their weak acidity. Izumi et al. showed that the insoluble salt $Cs_{2.5}H_{0.5}[PW_{12}O_{40}]$ (Cs-TPA) is an active solid-acid catalyst for esterification and hydrolysis [20]. Timofeeva et al. found that the esterification of dipicolinic acid (DA) with butanol, which is a step for the synthesis of pharmaceuticals, is catalyzed by TPA and its insoluble salts [21]. Bulk and supported heteropoly acids are active catalysts for the esterification of acetic acid with ethanol [15]. Typically, supported acids are more active than bulk ones. Among the esters of esterification reaction products, isoamyl esters are flavour esters, which have commercial value in the food industry (74,000 kg $year^{-1}$) because of their strong banana flavour [22,23].

In our previous reports, the catalytic behaviour of HPA/ZrO_2 has been studied for many acid-catalyzed reactions [24–29]. Recently, we have also demonstrated the catalytic activity of TPA/ZrO_2 supported over mesoporous silica MCM-41 and SBA-15 in acetylation of veratrole with acetic anhydride (AA) and Friedel-Crafts alkylation of phenol with benzyl alcohol under liquid phase conditions, respectively [30,31]. In order to perform a new contribution to the field of ecofriendly acid-catalyzed reactions, in this paper we report the results of esterification of isoamyl alcohol (IAA) with acetic acid (AA) using STA supported on mixed oxide like zirconia and mesoporous silica. The catalysts prepared by wet-impregnation techniques, have been unambiguously characterized by various sophisticated characterization techniques so as to study their physico-chemical properties and a correlation between the catalyst properties and the catalytic activity in the esterification reaction of IAA with AA in liquid phase conditions is reported.

2. Experimental

2.1. Materials

Hexadecyltrimethylammonium bromide (Aldrich, >99%) and triblock copolymer of ethylene oxide (EO) and propylene oxide (PO), $EO_{20}PO_{70}EO_{20}$ (Pluronic P123) (Aldrich, $M_{avg} = 5800$) were used as the structure directing templates. Tetraethylorthosilicate was purchased from Aldrich and used as the silica source. Zirconium oxychloride $ZrOCl_2{\cdot}8H_2O$ (99.5%) and 12-silicotungstic acid (STA) (99.9+ %) were obtained from Merck and used without further purification. Isoamyl alcohol (IAA) (≥99%), acetic acid (AA) (>99%) and all other alcohols and acids were procured from Aldrich. Zeolites with (SiO_2/Al_2O_3 ratio), H-beta (30), H-ZSM-5 (60) and H-Y (13.5) were obtained from Catalysis Pilot Plant (CPP-NCL, Pune). H-Mordenite (20) was obtained from PQ Zeolites BV, The Netherlands. All catalysts used in the reactions were in the powder form and were activated prior to their use in the reaction.

2.2. Catalyst synthesis

Pure siliceous SBA-15, MCM-41 and MCM-48 were synthesized according to the procedure reported in the literature [32–34] and STA/ZrO_2/MS composite materials were prepared by following procedure described [30]. The supported catalysts were prepared in two steps: (1) pure siliceous SBA-15 was impregnated with an aqueous solution of $ZrOCl_2{\cdot}8H_2O$ with a predetermined ZrO_2:SBA-15 (22.4%) (w/w) and the same amount of zirconia loading was used over MCM-41, which corresponded to monolayer coverage [35]. The resulting mixture was stirred in a rotary evaporator for 2–3 h followed by evaporation to dryness. The resultant solid was recovered, dried at 373 K for 12 h and powdered well for further use. (2) A series of catalysts with different STA loadings were prepared by suspending a known amount of an aqueous solution of STA (10–12 ml distilled water) per 1 g of dried ZrO_2/SBA-15 support. This mixture was stirred in a rotary evaporator for 2–3 h followed by evaporation to dryness and the samples were dried at 373 K for 12 h, powdered and calcined at 1123 K in air for 4 h. STA/ZrO_2 supported over MCM-41 and MCM-48 were also synthesized by the similar procedure used for SBA-15.

For studying the effect of addition of zirconia on the catalytic activity of STA/ZrO_2 supported mesoporous silica, a catalyst without ZrO_2 was synthesized by impregnating aqueous solution of 3.36 wt.% STA over SBA-15 using the similar procedure described as above. The effect of addition of STA was studied by synthesizing a catalyst without STA, which was prepared by impregnating 22.4 wt.% zirconia over SBA-15. The solvent was evaporated to dryness followed by drying and calcination at 1123 K for 4 h. Neat 15 wt.% STA/ZrO_2 was synthesized by mixing aqueous solutions of STA with zirconium oxychloride and then the solvent was evaporated using a rotary evaporator. The resulting material was collected, dried and calcined at 1123 K in air for 4 h. For comparison, TPA supported on mesoporous silica (TPA/MS) and TPA supported on functionalized mesoporous silica (TPA/MS-F) were synthesized using the procedure found in the literature [5].

2.3. Characterization of the catalysts

Zr, W and Si contents in the resulting solids were independently determined by inductively coupled plasma-optical emission spectroscopy (ICP-OES) and X-ray fluorescence spectrophotometer (Rigaku 3070 E Model with Rh target). The powder X-ray diffraction patterns were obtained on a Bruker small-angle X-ray scattering (SAXS) instrument with general area detector diffraction (GADDS) using Cu Kα radiation with a 2θ step size of 0.01°. SAXS pattern of the samples was collected in reflection mode using a Rigaku Dmax 2500 diffractometer with Ni filtered copper radiation. The diffractograms were recorded in the 2θ range of 0.5–10° with a 2θ step size of 0.01° and a step time of 1 s. The wide angle X-ray diffractograms were obtained on a Rigaku Model D/MAXIII VC, Japan, with

Cu Kα radiation 0.154 nm. The diffractograms were recorded in the 2θ range of 10–80° with a 2θ step size of 0.05° and a step time of 1 s. The crystallite size of the various samples was estimated from integral line width using the Scherrer relationship [36]. The nitrogen adsorption–desorption isotherms were measured at 77 K on an Omnisorb 100CX (Coulter, USA) analyzer. The specific surface area was calculated using the Brunauer–Emmett–Teller (BET) method. The pore size distributions were obtained from the adsorption branch of the nitrogen isotherms by Barrett–Joyner–Halenda method. HRTEM images were obtained with JEOL Model 1200 EX instrument operated at an accelerating voltage at 120 kV. The preparation of samples for HRTEM analysis involved sonication in isopropanol for 2–5 min and deposition on a copper grid. The Raman spectra were collected on a Brucker FRA106, equipped with a neodymium:yttrium aluminium garnet (Nd:YAG) laser that is frequency doubled to 532 nm. The spectra were recorded in the air atmosphere at room temperature using the laser power of 20 mW. For each spectrum, eight scans were collected in the 0–4000 cm^{-1} region, with the resolution of 5 cm^{-1}. ^{29}Si-MAS NMR and ^{1}H MAS NMR spectra were obtained on Bruker DRX-500 MHz and Bruker DSX-300 MHz spectrometer, respectively.

The acidity of the catalysts was estimated by temperature programmed desorption (TPD) of NH_3 on Micromeritics AutoChem 2910 instrument. About 0.1 g of the catalyst sample was dehydrated at 773 K in dry air for 1 h, purged with helium for 0.5 h. Then, the sample was cooled down to 398 K under the flow of helium and then 0.5 ml NH_3 pulses was supplied to the samples until no more uptake of NH_3 was observed. NH_3 was desorbed in a He flow by increasing the temperature to 813 K with a heating rate of 10 K min^{-1} measuring NH_3 desorbed by TCD.

The nature of acid sites (Brönsted and Lewis) of the catalyst samples with different loadings was characterized by in situ FT-IR spectroscopy with chemisorbed pyridine in drift mode on a FT-IR-8300 Shimadzu SSU-8000 instrument by averaging 500 scans with a resolution of 4 cm^{-1}. Prior to the analysis, the calcined powder samples were heated in situ from room temperature to 673 K with a heating rate of 5 K min^{-1} in a flowing stream (40 ml min^{-1}) of pure N_2. The samples were kept at 673 K for 3 h and then cooled down to 373 K. Thereafter, the pyridine vapors (20 μl) were introduced under N_2 flow and the IR spectra were recorded at different temperatures up to 673 K.

2.4. Esterification of isoamyl alcohol (IAA) by acetic acid (AA)

The esterification of IAA by AA has been used as a probe reaction for studying the activity of the catalysts. The schematic representation of the reaction and the detailed mechanism of proposed reaction are shown in reactions A and B in Scheme 1, respectively. The reaction was carried out in a 50 ml round-bottomed flask under continuous stirring equipped with condenser, a nitrogen inlet for maintaining an inert atmosphere, and an additional port for sample withdrawal. Temperature was maintained by placing the above assembly in a thermostatted

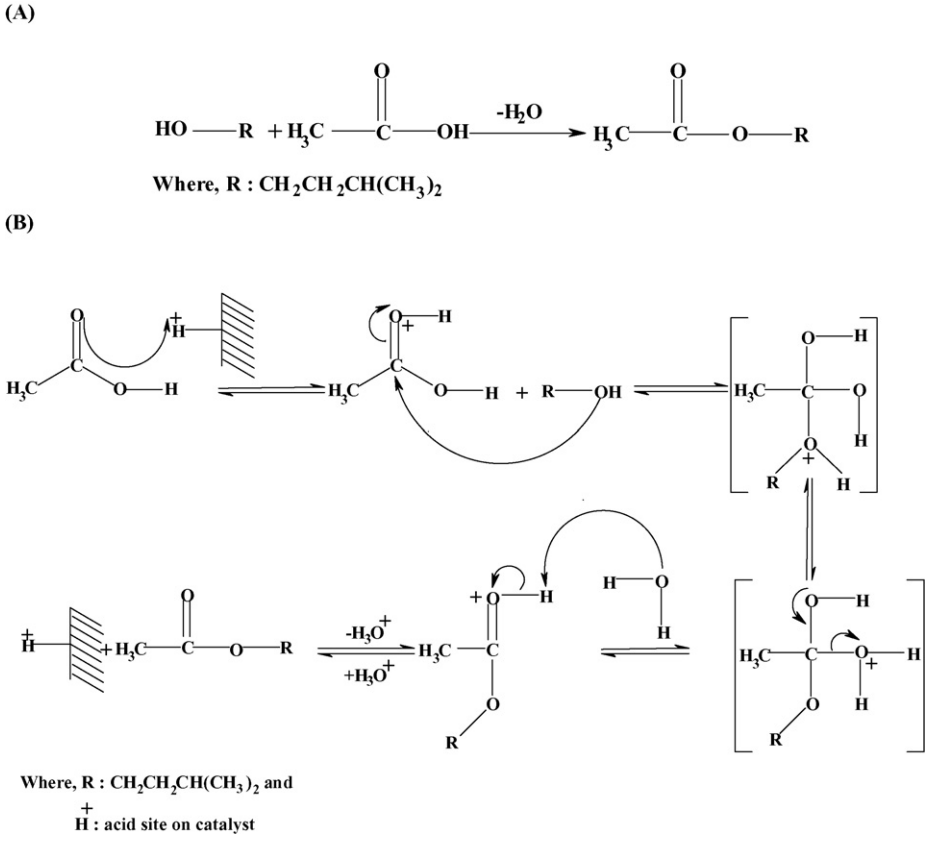

Scheme 1.

oil bath. The reaction was carried out at selected reaction conditions (373 K with a acid to alcohol molar ratio of 2 and the catalyst amount of 5 wt.% of total reaction mixture). Clear liquid samples withdrawn periodically were analyzed using a gas chromatograph (GC) with a SE-52 capillary column and a FID detector. The conversions were based on the consumed IAA in the reaction mixture. The products identifications were achieved by GC-MS and GC-IR.

3. Results and discussion

3.1. Characterization of the catalysts

The ratio of Si and W in 15 wt.% STA/22.4 wt.% ZrO_2/SBA-15 corresponding per Keggin unit obtained from XRF method and ICP-OES analysis was found to be 12.13 and 12.07, respectively. The small angle X-ray powder diffraction patterns of the catalysts with different (%) STA loadings calcined at 1123 K and 15 wt.% STA/22.4 wt.% ZrO_2/SBA-15 calcined at different temperatures are shown in Fig. 1A and B, respectively. It is seen from Fig. 1A that the structural order of the STA/22.4 wt.% ZrO_2/SBA-15 remained intact upto 30 wt.% of STA loading and started to loose upon further loading of STA. The wide-angle XRD patterns displayed three well-defined peaks at $2\theta \sim 30^\circ$, 50° and 60°, which are indexed to (1 1 1), (2 0 2) and (1 3 1) reflections, characteristics of tetragonal ZrO_2 (t-ZrO_2) phases. Also 15 wt.% STA/22.4 wt.% ZrO_2/SBA-15 catalyst shows intact mesoporosity even after calcination at 1273 K. The wide-angle XRD patterns of STA/22.4 wt.% ZrO_2/SBA-15 with different STA loading calcined at 1123 K is also shown in Fig. 1A (inset). It is interesting to see that the peaks related to tetragonal phase of zirconia are only appeared upto 15 wt.% STA loading, i.e. up to a monolayer coverage. After the monolayer coverage, the peaks corresponding to the WO_3 crystallites are appeared which could be mainly due to partial decomposition of STA.

The 15 wt.% STA/22.4 wt.% ZrO_2/SBA-15 sample calcined at different temperatures exhibits three well-resolved peaks which can be indexed to the (1 0 0), (1 1 0) and (2 0 0) reflections of the hexagonal space group *p6mm*. This indicates that the hexagonal mesoscopic structure of the materials is retained even after the calcination at very high temperature. It is important to note that the tetragonal phase along with WO_3 crystallites is observed in the catalyst after calcination above 1123 K as shown in inset of Fig. 1B. It is seen from Fig. 1B that the addition of 15 wt.% STA in 22.4 wt.% ZrO_2/SBA-15 supports the stabilization of the tetragonal phase of zirconia inside mesopores of SBA-15, which is imperative for preventing the growth of the particle size larger than the pore size of the support. The wide-angle XRD patterns of pure STA, pure ZrO_2, 15 wt.% STA/ZrO_2, 3.36 wt.% STA/SBA-15 and 22.4 wt.% ZrO_2/SBA-15 calcined at 1123 K are shown in Fig. 1C. It can be seen that ZrO_2 calcined at 1123 K exhibits both monoclinic and tetragonal phases of ZrO_2 where as 15 wt.% STA/ZrO_2 calcined at 1123 K possesses monoclinic and tetragonal phases of zirconia

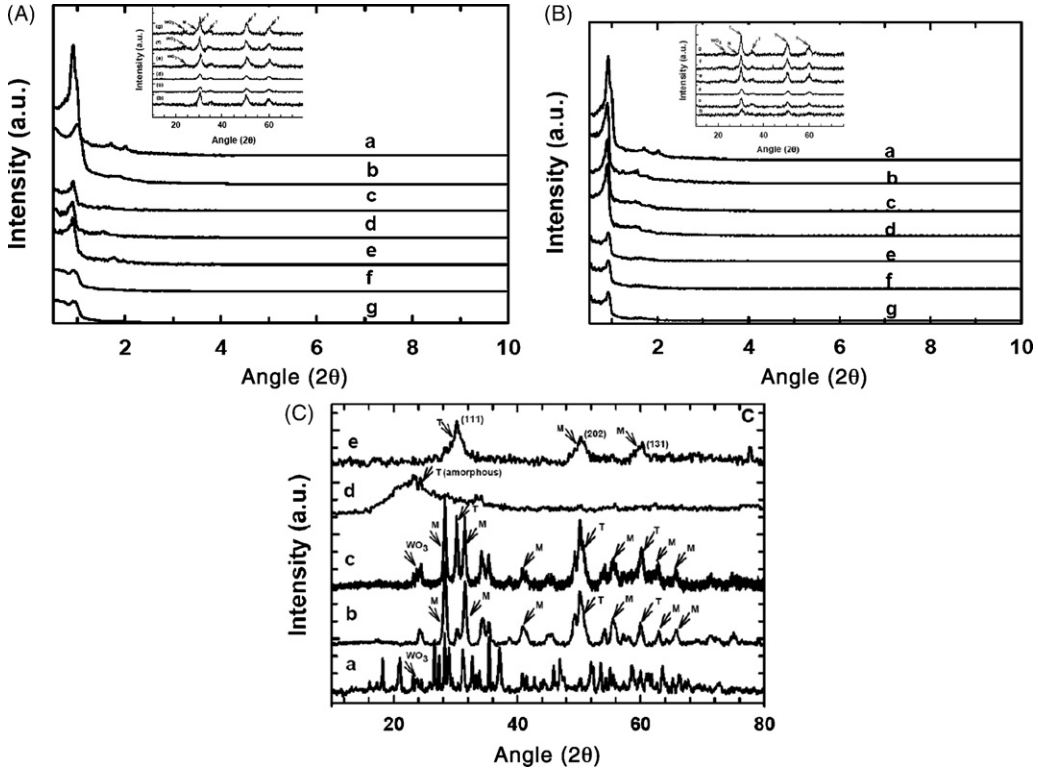

Fig. 1. (A) Low-angle powder XRD patterns of 22.4 wt.% ZrO_2/SBA-15 with different loadings of STA calcined at 1123 K: (a) pure SBA-15, (b) 5 wt.% STA, (c) 15 wt.% STA, (d) 20 wt.% STA, (e) 50 wt.% STA, (f) 70 wt.% STA and (g) 90 wt.% STA (inset: wide angle XRD patterns of the corresponding samples), (B) low-angle XRD patterns of 15 wt.% STA/22.4 wt.% ZrO_2/SBA-15 calcined at different temperature: (a) pure SBA-15, (b) 923 K, (c) 1023 K, (d) 1123 K, (e) 1173 K, (f) 1223 K and (g) 1273 K (inset: wide angle XRD patterns of the corresponding samples), (C) wide-angle XRD patterns of the samples calcined at 1123 K: (a) pure STA, (b) pure ZrO_2, (c) 15 wt.% STA/ZrO_2, (d) 3.36 wt.% STA/SBA-15 and (e) 22.4 wt.% ZrO_2/SBA-15.

Table 1
Physico-chemical properties and the catalytic activities STA/ZrO_2 supported SBA-15

STA/ZrO_2/SBA-15		SA[a] ($m^2\ g^{-1}$)	PV[b] ($cm^3\ g^{-1}$)	PD[c] (Å)	TA[d]	B	L	B/L	IAA conversion (%)	Rate constant $\times 10^{-5}$ (s^{-1})
STA (wt.%)	ZrO_2 (wt.%)									
5	22.4	396	0.63	65.7	0.29	0.06	0.06	1.00	27	2.91
15	22.4	372	0.61	65.3	0.40	0.10	0.07	1.42	50	6.42
30	22.4	334	0.58	65.1	0.35	0.08	0.07	1.15	41	4.89
50	22.4	333	0.54	64.7	0.30	0.066	0.06	1.10	30	3.30
70	22.4	200	0.34	64.4	0.27	0.041	0.05	0.82	20	2.07
90	22.4	200	0.31	63.7	0.22	0.028	0.05	0.56	14	1.39

All catalysts were calcined at 1123 K. Reaction conditions: IAA, 1.27 g; AA, 1.73 g; catalyst, 0.15 g; reaction temperature, 373 K; reaction time, 3 h.
[a] Surface area.
[b] Pore volume.
[c] Pore diameter.
[d] Total acidity (mmol g^{-1}).

and WO_3 crystallites due to decomposition of STA. However, 22.4 wt.% ZrO_2/SBA-15 exhibits only broad tetragonal zirconia phase while only amorphous phase is noticed for 3.36 wt.% STA/SBA-15.

The textural properties of STA/22.4 wt.% ZrO_2/SBA-15 with different loading of STA and 15 wt.% STA/22.4 wt.% ZrO_2/SBA-15 calcined at different temperatures are presented in Tables 1 and 2, respectively. It should be noted that the surface area, pore size and pore volume of STA/22.4 wt.% ZrO_2/SBA-15 are much lower than those of parent SBA-15 and decrease with increasing the loading of STA. This indicates that STA/ZrO_2 particles are well dispersed inside the mesochannels of SBA-15 support. The surface area and pore volume of the samples are also decreased drastically when the loading of STA is above 50 wt.%. This may be due to the fact that a low loading of STA enhances the interaction with the support, which may increase the surface diffusion of zirconia and inhibit sintering and stabilize the tetragonal phase of zirconia resulting in a small reduction in the surface area and pore volume. When the loading of STA is high, the formation of crystalline WO_3 is enhanced which most likely narrowed or plugged the pores of the samples leading to large reduction in the textural parameters. It is clear from Table 2 that the surface area, pore size and pore volume of 15 wt.% STA/22.4 wt.% ZrO_2/SBA-15 decrease with increasing the calcination temperature. Interestingly, a remarkable reduction is observed when the calcination temperature is above 1123 K. It is also important to note that the surface area of modified MCM-41 and MCM-48 (Table 3) is lower than that of the parent samples but much higher as compared to that of the modified SBA-15 samples, which could be mainly due to the incomplete filling of the STA/ZrO_2 inside the channels of MCM-41 and MCM-48 because of their small pore diameter.

TEM measurements were carried out to study the texture of the parent SBA-15 and 15 wt.% STA/22.4 wt.% ZrO_2/SBA-15 and the images are shown in Fig. 2a and b. It is clearly evident from the HRTEM images that STA/ZrO_2 particles with very small particle size are mainly dispersed inside the mesochannels of SBA-15 and the structural order of the material is remained intact even after calcination at 1123 K. The particle size of the material calculated from HRTEM analysis indicates that nanosized STA/ZrO_2 particles with the diameter of 4–5 nm is formed after wet impregnation over 15 wt.% of STA and 22.4 wt.% ZrO_2 in SBA-15 calcined at 1123 K.

^{29}Si MAS NMR and ^{1}H MAS NMR spectra of 15 wt.% STA/22.4 wt.% ZrO_2/SBA-15 are displayed in Fig. 3A and B, respectively. ^{29}Si MAS NMR shows two broad peaks centered at −100 and −110 ppm which can be attributed to $SiOH(OSi)_3$ environment (Q^3) species and $Si(OSi)_4$ environment (Q^4), in which silicon is covalently bound to four silicon atom via oxygen bridges, respectively [37]. Moreover, the broadness of the

Table 2
Effect of calcination temperature on the textural parameter and the catalytic activity of 15 wt.% STA/22.4 wt.% ZrO_2/SBA-15

Calcination temperature	SA[a] ($m^2\ g^{-1}$)	PV[b] ($cm^3\ g^{-1}$)	PD[c] (Å)	TA[d]	B	L	B/L	IAA conversion (%)	Rate constant $\times 10^{-5}$ (s^{-1})
873	484	0.67	69.8	–	0.012	0.027	0.44	0	Nil
923	472	0.64	67.0	0.25	0.03	0.055	0.55	14	1.39
1023	412	0.62	66.7	0.31	0.067	0.061	1.10	31	3.44
1123	372	0.61	65.3	0.40	0.10	0.07	1.42	50	6.42
1173	325	0.48	64.9	0.34	0.077	0.066	1.17	28	4.23
1223	250	0.43	64.4	0.30	0.042	0.065	0.65	12	3.04
1273	210	0.32	63.7	0.12	0.026	0.065	0.40	12	1.18

Reaction conditions: IAA, 1.27 g; AA, 1.73 g; catalyst, 0.15 g; reaction temperature, 373 K; reaction time, 3 h.
[a] Surface area.
[b] Pore volume.
[c] Pore diameter.
[d] Total acidity (mmol g^{-1}).

Table 3
Effect of different supports on esterification of IAA

Sample	SA[a] ($m^2\ g^{-1}$)	PV[b] ($cm^3\ g^{-1}$)	PD[c] (Å)	TA[d] acidity	B(L)	B/L	TOF $\times 10^{-1}$ (s^{-1})[e]	Rate constant $\times 10^{-5}$ (s^{-1})	IAA conversion (%)
SBA-15	929	1.36	73.3	–	–	–	–	–	–
MCM-41	1155	0.88	30.5	–	–	–	–	–	–
MCM-48	1096	0.71	26.1	–	–	–	–	–	–
22.4 wt.% ZrO_2/SBA-15	426	0.69	71.3	0.30	0.055 (0.059)	0.92	–	2.54	24
22.4 wt.% ZrO_2/MCM-41	589	0.38	27.7	0.24	0.039 (0.163)	0.24	–	0.88	9
22.4 wt.% ZrO_2/MCM-48	612	0.62	24.8	0.10	0.021 (0.21)	0.10	–	0.53	6
15 wt.% STA/ZrO_2/SBA-15	372	0.61	65.3	0.40	0.10 (0.070)	1.42	0.95	6.42	50
15 wt.% STA/ZrO_2/MCM-41	510	0.27	18.5	0.31	0.049 (0.245)	0.20	0.34	1.84	18
15 wt.% STA/ZrO_2/MCM-48	541	0.21	16.9	0.22	0.049	0.16	0.21	1.08	11
3.36 wt.% STA/SBA-15	340	0.59	69.9	0.27	0.030	0.85	0.36	1.95	19
15 wt.% STA/ZrO_2 (neat)	3	–	–	0.02	0.020	1.00	0.03	0.57	6

All catalysts were calcined at 1123 K except entry nos. 1–3. Entry 1: crystal size/nm (by TEM), 7.1; entry 4, ZrO_2 phase (tetragonal): crystal size/nm (by TEM), 5.5–6.5 and (by XRD), 6.1; entry 7, ZrO_2 phase (tetragonal): crystal size/nm (by TEM), 4–5 and (by XRD), 4.6. Reaction conditions: IAA, 1.27 g; AA, 1.73 g; catalyst, 0.15 g; reaction temperature, 373 K; reaction time, 3 h.

[a] Surface area.
[b] Pore volume.
[c] Pore diameter.
[d] Total acidity (mmol g^{-1}).
[e] TOF is calculated by considering three protons per Keggin unit (mol $mol^{-1}{}_{H^+}\ s^{-1}$).

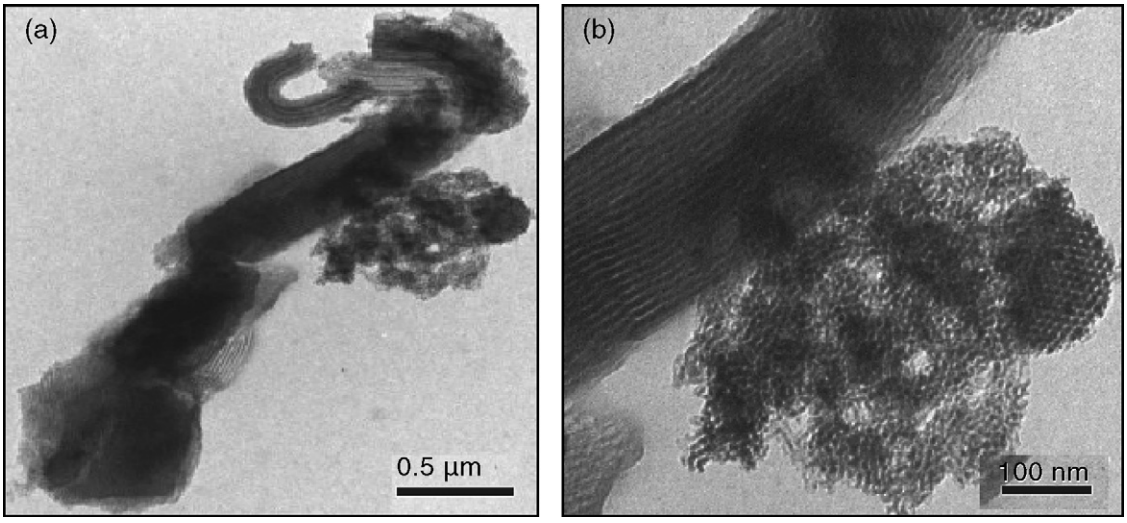

Fig. 2. HRTEM images of 15 wt.% STA/22.4 wt.% ZrO_2/SBA-15 calcined at 1123 K observed at different magnification: (a) 0.5 μm and (b) 100 nm.

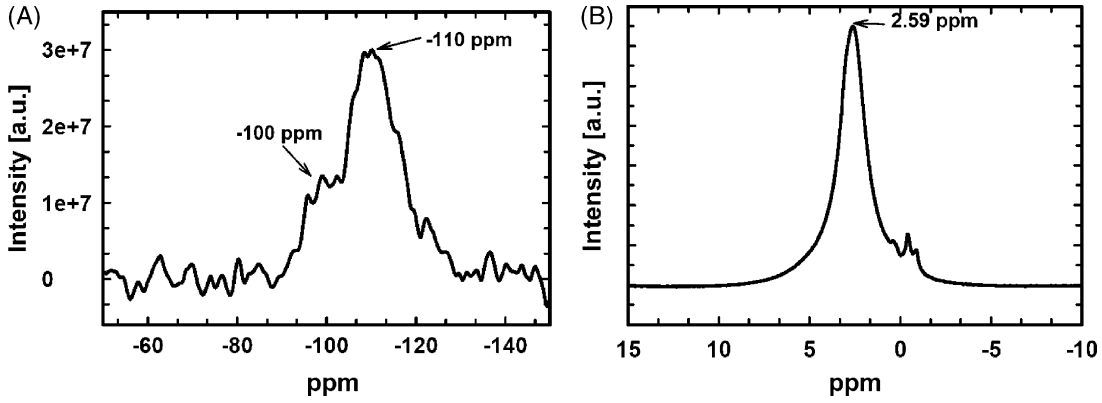

Fig. 3. (A) ^{29}Si MAS NMR and (B) ^{1}H MAS NMR spectra of 15 wt.% STA/22.4 wt.% ZrO_2/SBA-15 calcined at 1123 K.

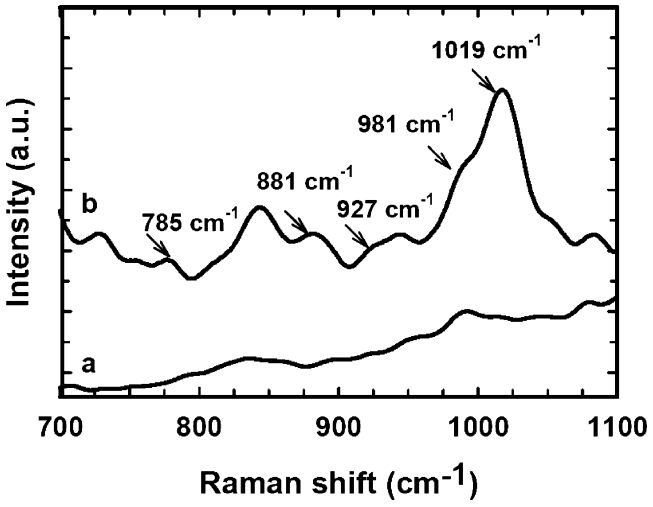

Fig. 4. FT-Raman spectra of: (a) 22.4 wt.% ZrO_2/SBA-15 and (b) 15 wt.% STA/22.4 wt.% ZrO_2/SBA-15 calcined at 1123 K.

^{29}Si signals has been attributed to the large distribution of the T–O–T angle [38]. ^{1}H MAS NMR spectrum shows a broad resonance around 2.6 ppm which could be attributed to the hydrogen bonding in silanol groups located inside the pore channels of SBA-15 support (Fig. 3B). Unfortunately, the ^{1}H signal at ca. 9 ppm which is typically seen for the neat STA is not observed in the STA modified SBA-15 [39]. This could be mainly due to a low loading of STA with respect to the silica support.

FT-Raman spectra of 22.4 wt.% ZrO_2/SBA-15 sample with and without STA calcined at 1123 K are presented in Fig. 4. Fifteen weight percent STA/22.4 wt.% ZrO_2/SBA-15 shows several bands centered around 1019, 981, 927, 881 and 785 cm^{-1}. The intense peak at 1019 cm^{-1} with a distinct shoulder at 981 cm^{-1} has been observed in STA by many authors and can be assigned to ν(W=O) symmetric and asymmetric stretching modes, respectively [40]. The band at 880 cm^{-1} could be assigned to the ν(W–O–W) asymmetric stretching mode. The broadening and minor shifts in the bands could be attributed to the formation of the species formed by linking the Keggin units to the zirconia support.

The NH_3–TPD profile for the catalysts 22.4 wt.% ZrO_2/SBA-15 and 15 wt.% STA/22.4 wt.% ZrO_2/SBA-15 calcined at 1123 K and its deconvoluted profile are shown in Fig. 5A and B, respectively. Both catalysts show a broad TPD profile, revealing that the surface acid strength is widely distributed. The total acidity of the catalysts with different STA loadings and calcined at different temperatures is also depicted in Tables 1 and 2, respectively. In addition, the total acidity of different catalysts was compared and the results are presented in Tables 2 and 3. It is evident from Table 1 that the acidity of STA/22.4 wt.% ZrO_2/SBA-15 increases with increasing the STA loading upto 15 wt.% and then decreases upon further loading. Moreover, the amount of ammonia desorption in the 15 wt.% STA/22.4 wt.% ZrO_2/SBA-15 catalysts calcined at different temperatures increases with increasing the calcination temperature and reaches a maximum at 1123 K. On further increase of the calcination temperature above 1123 K, the total acidity drastically decreases. This could be mainly due to decomposition of STA intoWO_3 crystallites. Therefore, it can be concluded that the Keggin-like unit of heteropoly acid retains its structure and acidity upto the STA loading of 15 wt.% while it decomposes partially into its oxides when the STA loading is increased above 15 wt.%.

It can be also seen from Fig. 5 that the amount of ammonia desorbed over 15 wt.% STA/22.4 wt.% ZrO_2/SBA-15 (Fig. 5A) is much lower as compared to that of 22.4 wt.% ZrO_2/SBA-15 catalyst. In order to get a clear picture on the TPD profiles, the ammonia desorption peaks are deconvoluted into two well resolved peaks using Gaussian function with temperature as variant [41]. The first peak centered around 440–450 K, referred as (type i), can be assigned to weak (structural) acid sites (Fig. 5B). The weak acid sites are originated from the anchored STA species. On calcination, the terminal W=O bonds of STA might react with partially dehydroxylated $(Zr(–O)_3)^+$ species to form anchored STA species (e.g., the formation of Zr–O–W bonds). These STA species would exert an electron-withdrawing effect on surface Zr^{4+} cations, making them to behave as Lewis acid sites. The peak (type ii) appeared in the range 520–540 K can be attributed to strong (Brönsted) acid sites which are originated during the calcination above 1123 K in which dehydroxylation

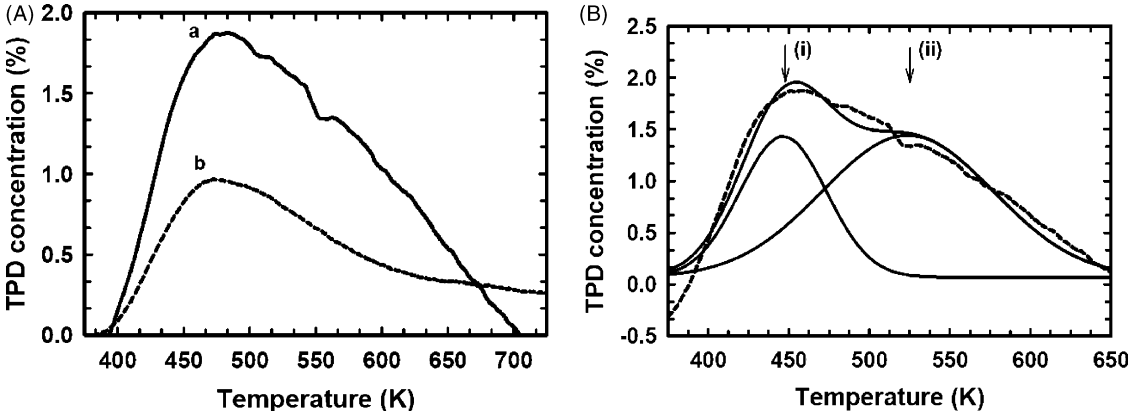

Fig. 5. NH_3–TPD profiles of: (A) 22.4 wt.% ZrO_2/SBA-15: (a) with 15 wt.% STA and (b) without STA and (B) 15 wt.% STA/22.4 wt.% ZrO_2/SBA-15 calcined at 1123 K.

of the support occurs. This process may weaken the interaction between the STA and zirconia and release free H^+ ions resulting in a higher Brönsted and total acidity.

The IR spectroscopy was used to quantity the amount and the type of the acid sites. The Brönsted to Lewis acid ratio (B/L) ratio calculated from the peak intensities of FT-IR pyridine adsorption spectra of STA/22.4 wt.% ZrO_2/SBA-15 with different STA loadings calcined at 1123 K and 15 wt.% STA/22.4 wt.% ZrO_2/SBA-15 catalysts calcined at different temperatures is given in Table 1. It is clearly seen from Table 1 that the B/L ratio increases with increaseing STA loading up to 15 wt.%, but then decreases with further increase of STA loading. At low loading, the catalyst exhibits mainly Lewis acidity, which decreases with increasing the STA loading whereas Brönsted acidity increases and reaches a maximum at 15 wt.% STA loading. The increase of STA loading above 15 wt.% also decreases the Brönsted acidity. The decrease in acidity above 15 wt.% could be due to the decomposition of STA, which exceeds monolayer coverage at higher STA loadings and forms crystalline WO_3, which prevents the accessibility of pyridine to the active sites. This confirms that 22.4 wt.% ZrO_2/SBA-15 sample with 15 wt.% STA has the highest acidity, which could be mainly due to the monolayer coverage of STA on finely dispersed ZrO_2 in SBA-15 channels. Apart from STA loading, the calcination temperature has a dramatic effect on the nature and amount of acid sites in the catalyst (Table 2). Brönsted acidity increases with increasing calcination temperature up to 1123 K (due to monolayer coverage) and then decreases with the further increase of the calcination temperature above 1123 K. On the other hand, the catalyst shows mainly Lewis acidity with a low Brönsted acidity at a low calcination temperature (823 K).

3.2. Catalytic activity

The liquid phase esterification of isoamyl alcohol (IAA) with acetic acid (AA) was carried out using STA/22.4 wt.% ZrO_2/SBA-15 with different loading of STA calcined at 1123 K and 15 wt.% STA/22.4 wt.% ZrO_2/SBA-15 calcined at different temperature and the results are presented in Tables 1 and 2, respectively. Esterification of IAA with 15 wt.% STA/22.4 wt.% ZrO_2/SBA-15 calcined at 1123 K catalyst under selected reaction conditions gave 50% IAA conversion with 100% selectivity for isoamyl acetate. Turn over frequency (mol $mol^{-1}_{H^+}$ s^{-1}) (by considering three protons per Keggin unit) and rate constant (s^{-1}, by considering esterification of IAA as a pseudo-first-order reaction) of 15 wt.% STA/22.4 wt.% ZrO_2/SBA-15 calcined at 1123 K in the esterification of IAA are found to be 0.0095 mol $mol^{-1}_{H^+}$ s^{-1} and 6.42×10^{-5} s^{-1}, respectively (Table 3). It is interesting to note that the TOF of the catalyst decreases with the increase of STA loading from 5 to 90 wt.% as shown in Fig. 6A. The effect of calcination temperature on 15 wt.% STA/22.4 wt.% ZrO_2/SBA-15 catalyst in its performance in esterification of IAA by AA is also displayed in Fig. 6B. There is an increase in IAA conversion upto 1123 K calcination temperature but decreases upon increasing the calcination temperature above 1123 K. This observation is supported by the fact that 15 wt.% STA/22.4 wt.% ZrO_2/SBA-15 calcined at 1123 K has a high B/L ratio and maximum concentration of acid sites, where STA forms a monolayer coverage over the support.

The catalytic activities of 22.4 wt.% ZrO_2/MCM-41 and 22.4 wt.% ZrO_2/MCM-48, with and without 15 wt.% STA were evaluated in the esterification of IAA with AA under identical reaction conditions and the results are compared with the catalytic activity of 15 wt.% STA/ZrO_2 and 22.4 wt.% ZrO_2/SBA-15 (with and without 15 wt.% STA) calcined at 1123 K (Table 3). It is evident from the results that 15 wt.% STA/ZrO_2 calcined at 1123 K gave the poorest conversion, which is at least eight times lower as compared to that of 15 wt.% STA/22.4 wt.% ZrO_2/SBA-15 calcined at 1123 K under the same reaction conditions. The enhancement in activity of 15 wt.% STA/22.4 wt.% ZrO_2/SBA-15 calcined at 1123 K is attributed to a large number of acid sites, high surface area and large pore diameter of the supports, which help the easy access of the acidic protons for the reactant molecules. It is also observed that 3.36 wt.% STA/SBA-15 and 22.4 wt.% ZrO_2/SBA-15 calcined at 1123 K also show a very low activity, which is mainly due to the lack of acidity which is highly required for the acid catalyzed reactions. In the present catalyst system, only zirconia loaded catalyst, i.e. 22.4 wt.% ZrO_2/SBA-15 calcined at 1123 K shows rather higher activity while the activity of the catalyst

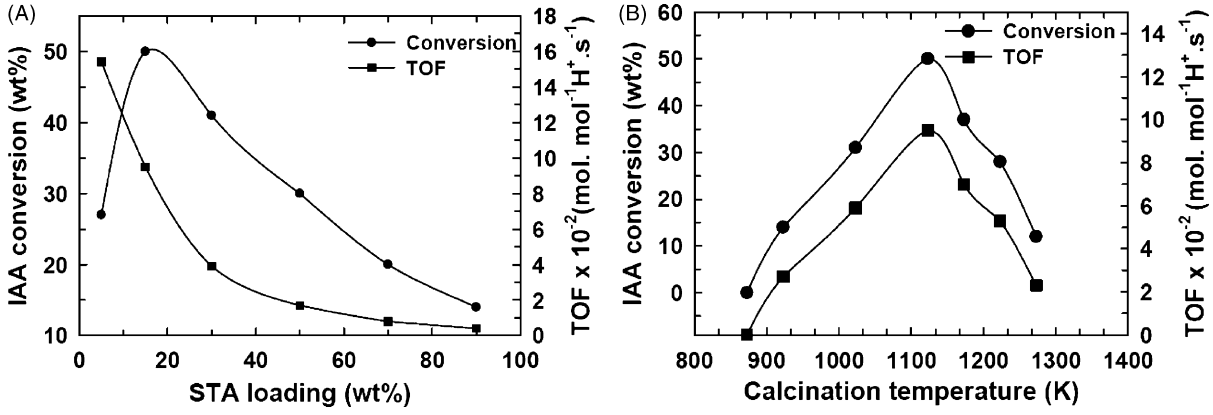

Fig. 6. (A) Effect of STA loading on IAA conversion and TOF over STA/22.4 wt.% ZrO_2/SBA-15 catalysts calcined at 1123 K. (B) Effect of calcination temperature on IAA conversion and TOF over 15 wt.% STA/22.4 wt.% ZrO_2/SBA-15 (reaction conditions: temperature, 373 K; AA to IAA (molar ratio), 2; catalyst weight, 0.15 g (5 wt.% of total reaction mixture); time, 3 h).

Table 4
Comparison of the activity of the catalysts in the esterification of IAA

Sample (Si/Al ratio)	Surface area ($m^2\ g^{-1}$)	Total acidity (mmol g^{-1})	IAA conversion (%)	TOF $\times 10^{-1}$ (s^{-1})[a]	Rate constant $\times 10^{-5}$ (s^{-1})
15 wt.% STA/ZrO_2/SBA-15	372	0.40	50	0.95	6.42
H-Beta (30)	540	0.94	51	0.04	6.61
H-Y (13.5)	530	2.25	43	0.017	5.20
H-Mordenite (20)	490	0.72	29	0.016	3.17
H-ZSM-5 (60)	364	0.82	22	0.036	3.57
TPA/MS (0)	ne	ne	29	ne	3.17
TPA/MS-F (0)	ne	ne	34	ne	3.85
Reusability of the 15 wt.% STA/ZrO_2/SBA-15					
First cycle	–	–	50	0.95	6.42
Second cycle	–	–	50	0.95	6.42

ne, Not evaluated. Reaction conditions: IAA, 1.27 g; AA, 1.73 g; catalyst, 0.15 g; reaction temperature, 373 K; reaction time, 3 h.
[a] TOF is calculated by considering three protons per Keggin unit (mol $mol^{-1}{}_{H^+}\ s^{-1}$).

increases two-fold when 15 wt.% of STA is loaded on the surface of the catalyst (Table 3). Interestingly, the catalytic activity of 15 wt.% STA/22.4 wt.% ZrO_2/SBA-15 is also much higher as compared to that of 15 wt.% STA/22.4 wt.% ZrO_2/MCM-41 and MCM-48 catalysts calcined at 1123 K. This could be mainly due the large-sized STA/ZrO_2 clusters which might block the pore channels of MCM-41 and MCM-48 support, whose pore diameters are much smaller than that of SBA-15 support and suppress the catalytic activity.

The catalytic activities of different catalysts such as H-beta, H-Y, H-ZSM-5, H-mordenite, TPA/MS, TPA/MS-F and 15 wt.% STA/22.4 wt.% ZrO_2/SBA-15 calcined at 1123 K in the esterification of an IAA with AA under identical reaction conditions are compared and the results are depicted in Table 4. Among the zeolite catalysts, H-beta is more active than others due to its strong and medium acid sites followed by H-Y. Surprisingly, ZSM and H-mordenite register much lower activity as compared to that of other zeolites catalysts, which may be due to smaller pore size and one-dimensional porous structure, respectively. TPA/MS-F shows higher catalytic activity as compared with TPA/MS catalyst and thereby shows higher rate constant. The catalytic activity of 15 wt.% STA/22.4 wt.% ZrO_2/SBA-15 is almost similar to that of the highly active H-beta catalyst. Therefore, 15 wt.% STA/22.4 wt.% ZrO_2/SBA-15 calcined at 1123 K was chosen as the catalyst for further investigations on the esterification of IAA with AA.

The effect of catalyst concentration on IAA conversion was studied by varying catalyst concentration from 1 to 10 wt.% of the total weight of the reaction mixture and the results are shown in Fig. 7A. It can be obviously seen that IAA conversion increases from 16.4 to 70.1% with increasing the catalyst concentration up to 10 wt.%, while the selectivity for IAA is almost unchanged. The effect of the molar ratio of AA to IAA (n_{AA}/n_{IAA}) on the activity and the selectivity over 15 wt.% STA/22.4 wt.% ZrO_2/SBA-15 at the reaction temperature of 373 K, catalyst weight of 5 wt.% of total reaction mixture is shown in Fig. 7B. With increasing n_{AA}/n_{IAA} ratio from 0.3 to 3, the conversion of IAA increases from 39.9 to 75.6. The effect of temperature on conversion of IAA and product selectivity over 15 wt.% STA/22.4 wt.% ZrO_2/SBA-15 was studied in the temperature range 343–383 K and the results are shown in Fig. 8. It is seen that the conversion of IAA increases upto 72.3% with increasing the reaction temperature to 383 K where as the selectivity for isoamyl acetate is almost constant. Under the optimized reaction conditions, reaction temperature of 373 K, catalyst weight of 0.150 g (5 wt.% of total reaction mixture) and n_{AA}/n_{IAA} ratio of 2, the esterification of IAA with AA performed for the reaction time of 7 h and the results are shown in Fig. 9.

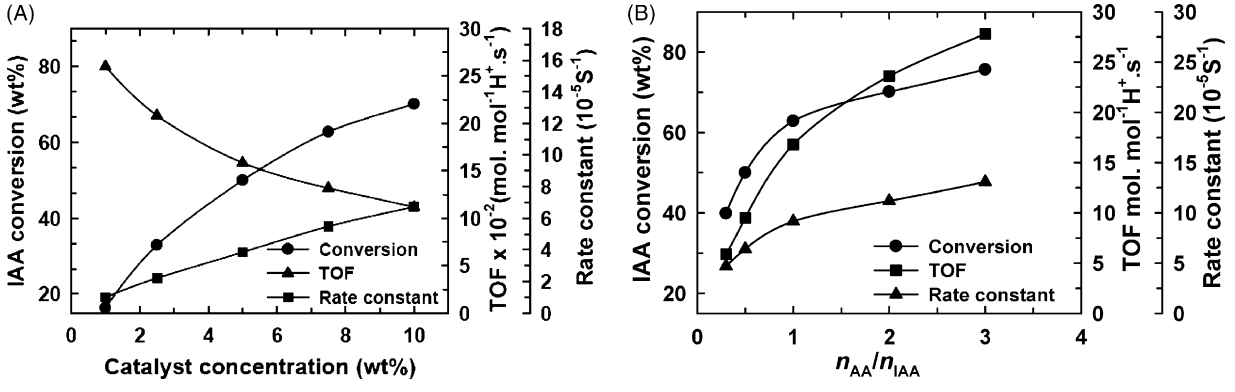

Fig. 7. (A) Effect of catalyst concentration on IAA conversion, TOF and rate constant over 15 wt.% STA/22.4 wt.% ZrO_2/SBA-15 calcined at 1123 K (reaction conditions: temperature, 373 K; AA to IAA molar ratio), 2; time, 3 h). (B) Effect of molar ratio on IAA conversion, TOF and rate constant over 15 wt.% STA/22.4 wt.% ZrO_2/SBA-15 calcined at 1123 K (reaction conditions: temperature, 373 K; catalyst weight, 0.15 g (5 wt.% of total reaction mixture); time, 3 h).

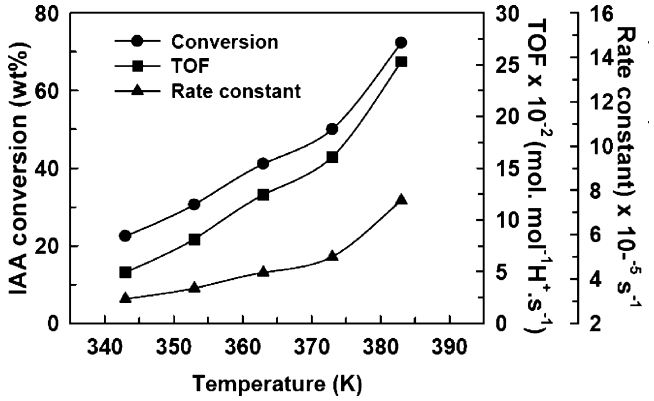

Fig. 8. Effect of temperature on IAA conversion, TOF and rate constant over 15 wt.% STA/22.4 wt.% ZrO_2/SBA-15 calcined at 1123 K (reaction conditions: AA/IAA (molar ratio), 2; catalyst weight, 0.15 g (5 wt.% of total reaction mixture); time, 3 h).

With increasing reaction time, the conversion of IAA increases to maximum of 83.12% with 100% selectivity for isoamyl acetate.

For catalyst reusability, the used catalyst in the first cycle of the reaction was separated by filtration, washed three times with 1,2-dichloromethane, dried in an oven at 373 K for 24 h, and activated at 773 K for 4 h in an air. The activated catalyst was used for esterification of IAA under the optimized reaction conditions. The procedure was repeated for the second cycle and the data on the conversion of IAA are presented in Table 4. From these results, it can be concluded that the catalyst can be reused as there is no appreciable loss in catalytic activity and product selectivity in the two cycles.

To check the leaching of STA into the reaction mixture, the reaction was carried out for 2 h under the optimized reaction conditions using fresh 15 wt.% STA/22.4 wt.% ZrO_2/SBA-15 calcined at 1123 K. The reaction was stopped, the catalyst was separated by filtration and then the filtrate was stirred for 1 h under the same reaction conditions. It was found that in the absence of the catalyst, there was no further increase in the conversion of IAA, indicating the absence of STA leaching into the reaction mixture. This observation also confirmed that the reaction was catalyzed heterogeneously. In addition, leaching

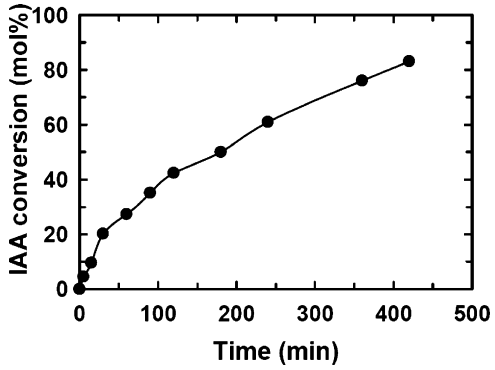

Fig. 9. Time-on-stream study over 15 wt.% STA/22.4 wt.% ZrO_2/SBA-15 calcined at 1123 K (reaction conditions: AA/IAA (molar ratio), 2; catalyst weight, 0.15 g (5 wt.% of total reaction mixture); time, 3 h).

of STA (i.e. dissolution of Si or W) into the hot filtrate was analyzed by inductively coupled plasma-optical emission spectroscopy (ICP-OES), which did not show the presence of Si or W in the filtrate.

The standard equation for a first-order series reaction, $C_A/C_{A0} = e^{-k_1 t}$, was used to determine the rate constant, where C_{A0} and C_A are the concentration of IAA at initial time and at time t, respectively. At one particular temperature, first-order rate constants were calculated at different reaction times and then the constant values of 'k_1' showed that the esterification of IAA is a first-order reaction. Energy of activation of the reaction was evaluated graphically. The activation energy (E_a) was obtained from an Arrhenius plot and a linear plot with negative slope equivalent to (E_a/R). The activation energy of was calculated to be 9.96 kcal mol^{-1}.

4. Conclusions

Nano-sized silicotungstic acid (STA) supported on zirconia embedded inside the various mesoporous silica such as SBA-15, MCM-41 and MCM-48 have been synthesized and unambiguously characterized by XRD, N_2 adsorption–desorption, TEM, ^{29}Si-MAS NMR, FT-Raman and the acidic behavior was studied by TPD of ammonia and FT-IR pyridine adsorption technique. The effect of calcination temperature and the loading of STA on the textural characteristics of the catalysts has also been studied and the results have been discussed. The results demonstrate that STA/ZrO_2 dispersed uniformly inside the mesopores of SBA-15 and the formation of nanosized (4–5 nm) STA/ZrO_2 particles inside the porous matrix of the support greatly depend on the percentage of STA loading, monolayer coverage on ZrO_2, geometry and nature of the mesoporous supports and calcination temperature. Catalytic activities have been correlated with the acidity of the catalysts. Effects of reaction parameters such as mole ratio of reactants, reaction temperature, catalyst concentration and reusability of the catalyst have been studied so as to get higher substrate conversions and product selectivities. Among mesoporous silica supports, SBA-15 was found to be the best support and provided higher thermal stability and catalytic activity than MCM-41 and MCM-48 in an esterification reaction. The mesoporous material has an advantage in the formation of nanosized and catalytically active STA/ZrO_2 by stabilizing zirconia in tetragonal phase at 1123 K, which provided higher catalytic activity than the neat STA/ZrO_2 in an esterification reaction. Among the catalysts, 15 wt.% STA/22.4 wt.% ZrO_2/SBA-15 calcined at 1123 K was found to be the most active and acidic catalyst, showing higher conversion and selectivity than neat 15 wt.% STA/ZrO_2 in esterification of IAA by AA. The reaction was found to be heterogeneously catalyzed and no contribution from homogeneous (leached) STA into the medium under the reaction conditions was observed.

Acknowledgements

This work was financially supported by DST-SERC, New Delhi. One of the authors (Dhanashri P. Sawant) acknowledges CSIR New Delhi for Senior Research Fellowship.

References

[1] A. Zaidi, J.L. Gainer, G. Carta, Biotechnol. Bioeng. 48 (1995) 601.
[2] R.C. Larock, Comprehensive Organic Transformations, second ed., VCH, New York, 1999.
[3] S. Hari Krishna, B. Manohar, S. Divakar, S.G. Prapulla, N.G. Karanth, Enzyme Microb. Technol. 26 (2000) 131.
[4] H. Ghamgui, M. Karra-Chaˆabouni, S. Bezzine, N. Miled, Y. Gargouri, Enzyme Microb. Technol. 38 (6) (2006) 788.
[5] M.D. Romero, L. Calvo, C. Alba, M. Habulin, M. Primožič, Ž. Knez, J. Supercrit. Fluids 33 (2005) 77–84.
[6] M. Rizzi, P. Stylos, A. Riek, M. Reuss, Enzyme Microb. Technol. 14 (1992) 709.
[7] L. Lian-sun, L. Ren-guey, Fluid Phase Equilib. 165 (1999) 261.
[8] A. Güvens, N. Kapucu, M. Ülkü, Process Biochem. 38 (2002) 379.
[9] L.R. Pizzio, P.G. Vázquez, C.V. Cáceres, M.N. Blanco, Appl. Catal. A: Gen. 256 (2003) 125.
[10] L.R. Pizzio, M.N. Blanco, Appl. Catal. A: Gen. 255 (2003) 265.
[11] A. Palani, A. Pandurangan, J. Mol. Catal. A: Chem. 226 (2004) 129.
[12] H.T.R. Teo, B. Saha, J. Catal. 228 (2004) 174.
[13] N. Bhatt, A. Patel, J. Mol. Catal. A: Chem. 238 (2005) 223.
[14] I.V. Kozhevnikov, Chem. Rev. 98 (1998) 171.
[15] Y. Izumi, K. Urabe, M. Onaka, Zeolite, Clay and Heteropoly Acid in Organic Reactions, Kodansha/VCH, Tokyo, 1992, pp. 99–161.
[16] C. Hu, M. Hashimoto, T. Okuhara, M. Misono, J. Catal. 143 (1993) 437.
[17] G.M. Maksimov, I.V. Kozhevnikov, React. Kinet. Catal. Lett. 39 (1989) 317.
[18] M.A. Schwegler, H. van Bekkum, N.A. de Munck, Appl. Catal. A: Gen. 74 (1991) 191.
[19] P. Dupont, F. Lefebvre, J. Mol. Catal. A: Chem. 114 (1996) 299.
[20] Y. Izumi, M. Ono, M. Ogawa, K. Urabe, Chem. Lett. (1993) 825.
[21] M.N. Timofeeva, R.I. Maksimovskaya, E.A. Paukshtis, I.V. Kozhevnikov, J. Mol. Catal. A: Chem. 102 (1995) 73.
[22] G. Langrand, C. Triantaphylides, J. Baratti, Biotechnol. Lett. 12 (8) (1988) 549.
[23] F.W. Welsh, W.D. Muray, R.E. Williams, Crit. Rev. Biotechnol. 9 (2) (1989) 105.
[24] D.P. Sawant, S.B. Halligudi, J. Mol. Catal. A: Chem. 237 (2005) 137–145.
[25] D.P. Sawant, B.M. Devassy, S.B. Halligudi, J. Mol. Catal. A: Chem. 217 (2004) 211.
[26] B.M. Devassy, G.V. Shanbhag, S.P. Mirajkar, W. Böhringer, J. Fletcher, S.B. Halligudi, J. Mol. Catal. A: Chem. 233 (2005) 141.
[27] B.M. Devassy, G.V. Shanbhag, F. Lefebvre, S.B. Halligudi, J. Mol. Catal. A: Chem. 210 (2004) 125.
[28] B.M. Devassy, F. Lefebvre, S.B. Halligudi, J. Catal. 229 (2005) 576.
[29] B.M. Devassy, S.B. Halligudi, J. Catal. 236 (2005) 313.
[30] D.P. Sawant, A. Vinu, N.E. Jacob, F. Lefebvre, S.B. Halligudi, J. Catal. 235 (2005) 341.
[31] D.P. Sawant, A. Vinu, F. Lefebvre, S.B. Halligudi, J. Mol. Catal. A: Chem. 262 (2007) 98–108.
[32] M. Hartmann, S. Racouchot, C. Bischof, Microporous Mesoporous Mater. 27 (1999) 309.
[33] K. Schumacher, M. Grün, K.K. Unger, Microporous Mesoporous Mater. 27 (1999) 201.
[34] D. Zhao, J. Sun, Q. Li, G.D. Stucky, Chem. Mater. 12 (2000) 275.
[35] J. He, X. Duan, C. Li, Mater. Chem. Phys. 71 (2001) 221.
[36] H.P. Klug, L.E. Alexander, X-ray Diffraction Procedures, Wiley, New York, 1974.
[37] D. Zhao, J. Feng, Q. Huo, N. Melosh, G.H. Fredrickson, B.F. Chmelka, G.D. Stucky, Science 279 (1998) 548.
[38] N. Chino, T. Okubo, Microporous Mesoporous Mater. 87 (2005) 15.
[39] W. Hu, Q. Luo, Y. Su, L. Chen, Y. Yue, C. Ye, F. Deng, Microporous Mesoporous Mater. 92 (2006) 22.
[40] A. Thomas, C. Dablemont, J.-M. Basset, F. Lefebvre, C. R. Chim. 8 (2005) 1969.
[41] A. Sakthivel, S.K. Badamali, P. Selvam, Microporous Mesoporous Mater. 39 (2000) 457.